Hindawi Publishing Corporation
Advances in Mechanical Engineering
Volume 2013, Article ID 329264, 9 pages
http://dx.doi.org/10.1155/2013/329264

Research Article

Experimental Characterisation and Modelling of Homogeneous Solid Suspension in an Industrial Stirred Tank

Sébastien Calvo, Angélique Delafosse, Marie-Laure Collignon, Michel Crine, and Dominique Toye

Laboratory of Chemical Engineering, University of Liège, 15 Allée du 6 Août, 4000 Liège, Belgium

Correspondence should be addressed to Sébastien Calvo; scalvo@ulg.ac.be

Received 8 April 2013; Accepted 27 May 2013

Academic Editor: Guan Heng Yeoh

In this work, we study the conditions needed to reach homogeneous distribution of aluminium salts particles in water inside a torispherical bottom shaped stirred tank of 70 L equipped with a Pfaudler RCI type impeller and three equispaced vertical baffles. The aim of the present study is to develop a CFD model describing the quality of particle distribution in industrial scale tanks. This model, validated with experimental data, is used afterwards to develop scale-up and scale-down correlations to predict the minimum impeller speed needed to reach homogeneous solid distribution Nhs. The commercial CFD software Fluent 14 is used to model the fluid flow and the solid particle distribution in the tank. Sliding Mesh approach is used to take the impeller motion into account. Assuming that the discrete solid phase has no influence on the continuous liquid phase behaviour, the fluid flow dynamics is simulated independently using the well-known k-ε turbulence model. The liquid-solid mixture behaviour is then described by implementing the Eulerian Mixture model. Computed liquid velocity fields are validated by comparison with PIV measurements. Computed Nhs were found to be in good agreement with experimental measurements. Results from different scales allowed correlating Nhs values to the volumetric power consumption.

1. Introduction

Suspension of solid particles in a liquid is a key aspect of many processes, such as dissolution, crystallisation, adsorption, desorption, and catalytic or enzymatic reactions. Solid dispersion inside a stirred tank is a physical process where particles or aggregates are maintained in suspension and dispersed through a fluid by the action of an impeller. The main objective of this process is to avoid particle accumulation near the tank bottom and to obtain a solid distribution as uniform as possible to ensure a good quality mixing, that is, a homogeneous distribution of all components (catalyser, reacts, and products) inside the tank [1].

Depending on the application, the aim of mixing solid-liquid system is to obtain a "complete" suspension or a "homogeneous" suspension. In most published works, authors describe the solid dispersion process in stirred tanks using the just-suspended speed Njs which is the minimum speed of rotation of the impeller for which no particle deposits on the tank bottom and thus for which particles are completely suspended [2, 3]. On the other hand, very few studies have described the stirring conditions for which the solid distribution is homogeneous in the whole tank. This is mainly due to the fact that small improvement in process performance is obtained by increasing agitation speed above Njs if compared to the corresponding increase of operating cost related to the dissipated power increase.

However, in some pharmaceutical and cosmetic processes, working with homogeneous suspensions is imperative. In this case, no correlation, similar to the Zwitering's one which allows the calculation of Njs [4], is available to predict the minimum impeller speed Nhs (homogeneous suspension speed) required to get an homogeneous distribution of solid particles. Experimental investigations and theoretical modelling are thus required to get robust scale-up and scale-down models allowing the prediction of Nhs. At the lab scale, several experimental methods allow the characterisation of solid dispersion in stirred tanks, such as electrical tomography [3], optical [5] or nephelometric probe [6], or direct visualisation of particle cloud [7]. In larger industrial vessels,

application of these methods may be problematic. Use of CFD codes, validated on the basis of experimental results collected at the lab scale, may be an appropriate alternative approach to characterise solid dispersion at the industrial scale.

During the last decade, computational fluid dynamics (CFD) has become a very powerful tool in the process industry not only for research and development of new processes but also for understanding and optimisation of existing ones. Number of authors have simulated turbulent fluid flow inside stirred tank, in many kinds of geometry and applications with commercial CFD codes (Fluent, CFX, ...). Reported results have shown the robustness of these codes to characterise the flow field in stirred tanks [8, 9]. Relevance of different simulation methods (LES, k-ε, RSM, ...) used to describe turbulent quantities has been studied [10, 11]. Considering their results, we decided to use the well-known k-ε model which allows sufficient accuracy on global turbulent quantities while keeping within a reasonable calculation time.

Concerning the modelling of the solid suspension, the literature mainly mentions two possible models: the "Eulerian Multiphase model" (MFM) and the "Eulerian Mixture model." In the Eulerian Multiphase model, continuity and momentum balance equations are solved for each phases. The Eulerian Mixture model is a simplified version of the Eulerian Multiphase model suitable for dilute suspensions and small particle Stokes number. In this model continuity and momentum balance equations are solved for one mixture phase, the hydrodynamics parameters of which are computed from mass-averaged properties of each phase. Only one equation for the transport of volume fraction is added and solved for the dispersed phase. Consequently the dispersed phase is transported as a passive scalar in the tank. Interphase coupling term allows taking into account the relative motion of the dispersed phase from the continuous phase. This term consists of four different interphase forces: lift force, Basset force, virtual mass force, and drag force. Due to the very small influence of lift, Basset, and virtual mass forces on the simulated solid hold-dup profile [12], only the drag force may be considered in the interphase momentum exchange term (Schiller-Naumann). Results obtained using these two models are available in the literature and show that the Eulerian Multiphase model [13–15] is more accurate than the Eulerian Mixture model [16, 17] when working with particle size higher than 100 μm and solid fraction ranging between 0.2 and 16%,. Nevertheless, the Eulerian Mixture model is less time consuming and well adapted for low particle size (<10 μm) and concentration (<0.1%) and should be suitable in our case.

2. Experimental Setup and Results

2.1. Stirred Tank. In the present work, experimental studies are performed in a pilot stirred tank of 70 L (Figure 1). It consists of a 430 mm diameter (D) and 516 mm height ($H/D = 1.2$) cylinder equipped with a torispherical bottom shape and three equispaced baffles with standard dimensions. Mixing is ensured by a 228 mm diameter ($d/D = 0.53$) Pfaudler RCI (Retreat Curve Impeller) type impeller placed close to the tank bottom (clearance $Y/D = 0.06$) in order to ensure a "single-loop" flow configuration. Working fluid

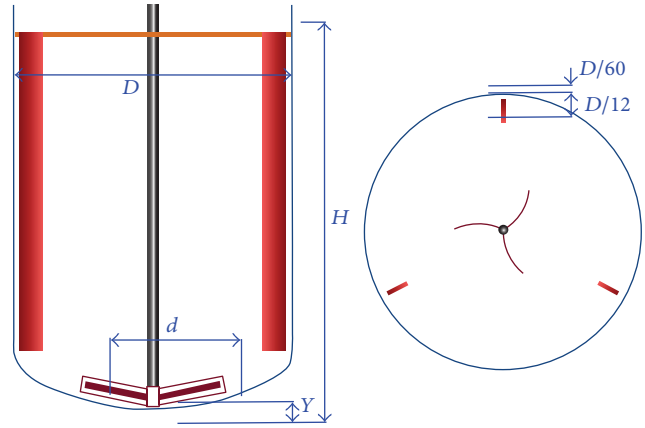

Figure 1: Schema of the pilot stirred tank.

is water in standard conditions ($\rho_l = 998\,\text{kg·m}^{-3}$ et $\mu_l = 10^{-3}\,\text{kg·m}^{-1}\text{·s}^{-1}$).

2.2. Solid Suspension. The solid phase used in this work is a mixture of aluminium salts (aluminium hydroxide and aluminium phosphate) commonly used in cosmetic and pharmaceutical processes. Only the properties of mixture will be considered in this study. Individual properties of each salt will not be taken into account. The density of the mixture is $2500\,\text{kg·m}^{-3}$ (ρ_s) and the total particle load corresponds to an average volume fraction of $0.74\,\text{cm}^3\text{·L}^{-1}$.

Size distribution of particles has been measured by LASER granulometry (Figure 2). This distribution has first been evaluated in a stirred cell. The measured mean particle size ranged between 5 and 7 μm. Stopping agitation inside the measurement cell allows the visualisation of formation of aggregates due to the hydration of aluminium salts. As can be seen in Figure 2, after 60 min without agitation, the mean size of particles reached 60 μm. Agitation resumption allows the breaking the aggregates and returning to the initial size of the particles. These results show that agitation has a significant influence on the particle size distribution with a tendency to reduce the average size.

The equivalent diameter of particle is a very commonly used quantity to describe their behaviour in suspension. It was determined by measuring their settling velocity, because, for a solid suspension composed of a wide range of particle sizes, an equivalent diameter can be expressed as a function of the particle settling velocity. The works of Perry and Green [18] give the correlation to express the settling velocity V_t for spherical particles:

$$V_t = \left(\frac{4 g d_P^2 (\rho_S - \rho_L)}{3 C_D \rho_L} \right)^{1/2}, \quad (1)$$

where g is the gravitational constant ($9.81\,\text{m·s}^{-2}$) and C_D represents the drag coefficient which is a function of particle Reynolds number Re_P and particles shape:

$$\text{Re}_P = \frac{\rho_L V_t d_P}{\mu}. \quad (2)$$

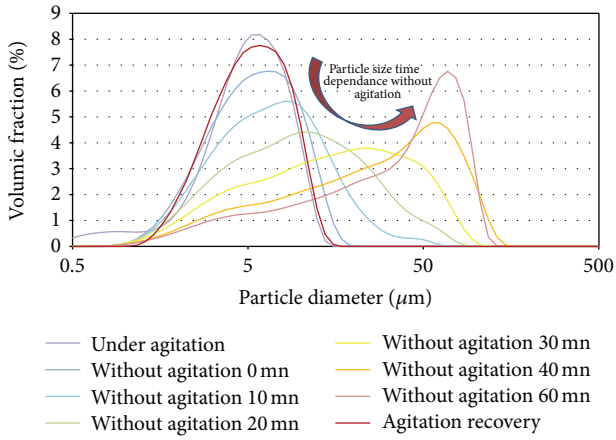

FIGURE 2: Particle size distribution and the impact of agitation on particle size.

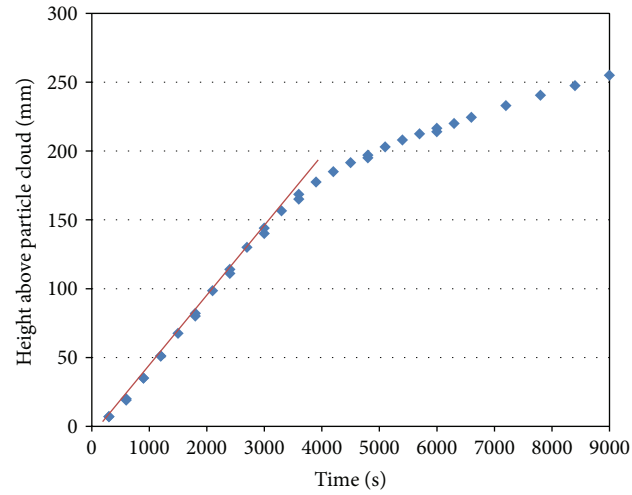

FIGURE 3: Time evolution of the particle sedimentation front: estimation of the settling velocity.

TABLE 1: Hydrodynamic regimes for settling particles.

Regime	Reynolds number	C_D Expression
Stokes' law (laminar)	$\mathrm{Re}_p < 0.3$	$C_D = 24/\mathrm{Re}_p$
Intermediate law	$0.3 < \mathrm{Re}_p < 1000$	$C_D = 18.5/\mathrm{Re}_p^{3/5}$
Newton's law (turbulent)	$1000 < \mathrm{Re}_p < 35 \times 10^4$	$C_D = 0.445$

Correlation for C_D covers several hydrodynamic regimes. The corresponding ranges for Re_P and the correlating expression of C_D are shown in Table 1 for three hydrodynamics regimes.

When the expressions for C_D are substituted in (1), the resulting expressions for the free settling velocity V_t are, respectively,

(i) for the Stokes' law (laminar) regime, $\mathrm{Re}_p \leq 0.3$:

$$V_t = \frac{g d_{P(\rho_S - \rho_L)}}{18\mu}, \quad (3)$$

(ii) for the Newton's law (turbulent) regime, $1000 \leq \mathrm{Re}_P \leq 35.104$:

$$V_t = 1.73\left[\frac{g d_{P(\rho_S - \rho_L)}}{\rho_L}\right]^{1/2}. \quad (4)$$

The settling velocity of the suspension has been estimated by observing the particle sedimentation front evolution inside a graduated tube (Figure 3). The settling velocity was found to be equal to 23 cm·h^{-1} which corresponds to an equivalent diameter of 9 μm considering that the particle flow regime was found to be ruled by the Stokes' law (laminar). If compared to the particle size distribution obtained by granulometry (Figure 2), this result shows that this size does not correspond to individual particles but corresponds to aggregates formed after the agitation stopped. Aggregates have also been observed visually during the particle sedimentation front study.

In the case of our solid phase (mixture of aluminium salts), the estimation of the equivalent diameter of the suspension in a stirred tank seems to be difficult because the particle size directly depends on the surrounding hydrodynamic conditions. In the CFD model, this information is a key parameter to model the solid suspension. Considering the complex behaviour of our solid phase, we decide to use a pragmatic approach. We supposed that the particles are spherical and an equivalent diameter will be fitted to be representative of the experimental observations. The fitted value of the equivalent diameter will then be compared with previous results to check the soundness of our approach.

2.3. Experimental Investigation of the Homogeneous Suspension Speed. Homogeneous suspension is reached when the particle concentration is uniformly distributed inside the stirred tank. In the case of particles denser than the working fluid, heterogeneity first appears at the top of the tank. Nhs has thus been measured by a nephelometric probe (Figure 4) disposed near the liquid free surface. The probe is placed one centimetre below the liquid free surface to avoid disturbances due to the surface deformation.

The experimental method consists of two steps. First, the agitation speed is fixed at a high value to obtain a steady nephelometric signal which corresponds to a homogeneous suspension ($N_{\mathrm{init}} \gg$ Nhs). The agitation speed is then decreased at a lower value (N_{test}) and the nephelometric signal stability is controlled. We considered here that homogeneous suspension speed Nhs is reached when the oscillation of the signal does not exceed 2% of the value obtained at N_{init}. These two steps ($N_{\mathrm{init}} - N_{\mathrm{test}}$) are then repeated increasing N_{test} value until Nhs is reached.

In this investigation, the position of the nephelometric probe remained constant and results may not be representative of the homogeneity in the entire volume of the tank. As

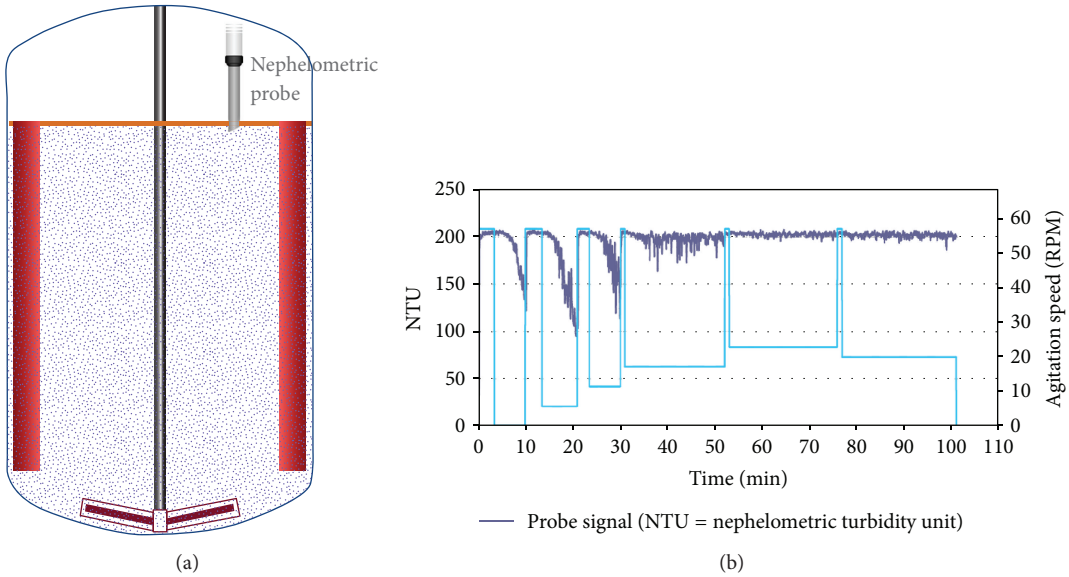

Figure 4: Experimental measurement of Nhs by nephelometric method.

nonhomogeneous zones were visually observed near the liquid free surface, we make here the hypothesis that measured Nhs corresponds to a homogeneous suspension within 95% of the tank volume. Assuming these considerations, Nhs was found to be equal to 20 RPM in the 70 L pilot tank.

3. CFD Modelling

3.1. Liquid Flow Model: k-ε. Geometry of the 70 L pilot tank and its meshing have been, respectively, performed with the commercial tools provide by Ansys Software "DesignModeler" and "Ansys Meshing" (Figure 5(a)). In order to use the Sliding Mesh (SM) method, two fluid zones were defined: an inner rotating cylindrical volume (4.3×10^{-3} m^3) centred on the impeller which includes a part of bottom wall (Y/D = 0.06) and an outer stationary zone (65.7×10^{-3} m^3), containing the rest of the tank and the baffles. The interface is located at equal distance from the impeller Tip and the inside edge of the baffles so that the region of flow periodicity was contained within the sliding mesh. To counterbalance the rotation of the wall below the impeller, a "moving wall" condition is set in the direction opposite to the impeller rotation.

The mesh used consists of approximately 125,000 and 375,000 hexahedrons for the rotating and the stationary zones, respectively. An illustration of the meshed zones is given in Figure 5(a), which clearly shows that finer meshes haves been used around the impeller and in the impeller discharge zone (inside the torispherical bottom), where the velocity spatial gradients are expected to be large. We also take care of keeping the same mesh dimension between the rotating and the stationary interface to ensure a good exchange of the hydrodynamic quantities between the two zones during the calculation. A "no-slip" condition is applied on all walls of the geometry. Assuming that the baffles limit the vortex formation, a symmetry condition was used at the liquid free surface.

Simulations of the turbulent single phase flow are then performed with the commercial CFD code Fluent 14 (Ansys 14) using the standard k-ε model [1]. The working fluid is water, with a density ρ_l = 998 kg·m^{-3} and a viscosity μ_l = 10^{-3} kg·m^{-1}·s^{-1}. As the SM method was used, the flow resolution is unsteady. At each time step, the position of the rotating zone relative to the stationary one is recomputed and the grid interface of the rotating zone slides along the interface of the stationary zone. For all simulations, the time step is set as a function of the impeller speed so that it rotates of a 2° angle per time step.

At the end of each time step, after a maximum of 20 iterations, the convergence criterion reaches 10^{-4} for the continuity and 10^{-5} for momentum and turbulence quantities. Simulations are performed in double precision with the segregated implicit solver. Temporal discretisation and spatial discretisation of all quantities (continuity, momentum and turbulence) are of the second order.

Finally, the analysis of the velocity field is performed after three or four complete revolutions of the impeller, when convergence of the Tip velocity is reached. For each time step, a velocity field is computed on a vertical plane which corresponds to one position of the impeller (phase average). To avoid the influence of the impeller position, an average is performed over a complete rotation of the impeller. The mean velocity field is thus obtained (Figures 5(b) and 5(c)).

3.2. Experimental Validation of the Turbulent Flow Model. Particle Image Velocimetry (PIV) is a nonintrusive optical technique which allows measuring instantaneous velocity fields in a plane of the flow. The 2D PIV technique is presented in Figure 6. To obtain the instantaneous velocity fields, fluid is previously seeded with fluorescent particles of the same density as the working fluid in order to follow the flow streamlines without disturbing it. The fluid is then highlighted by two light pulses provide by a vertical LASER

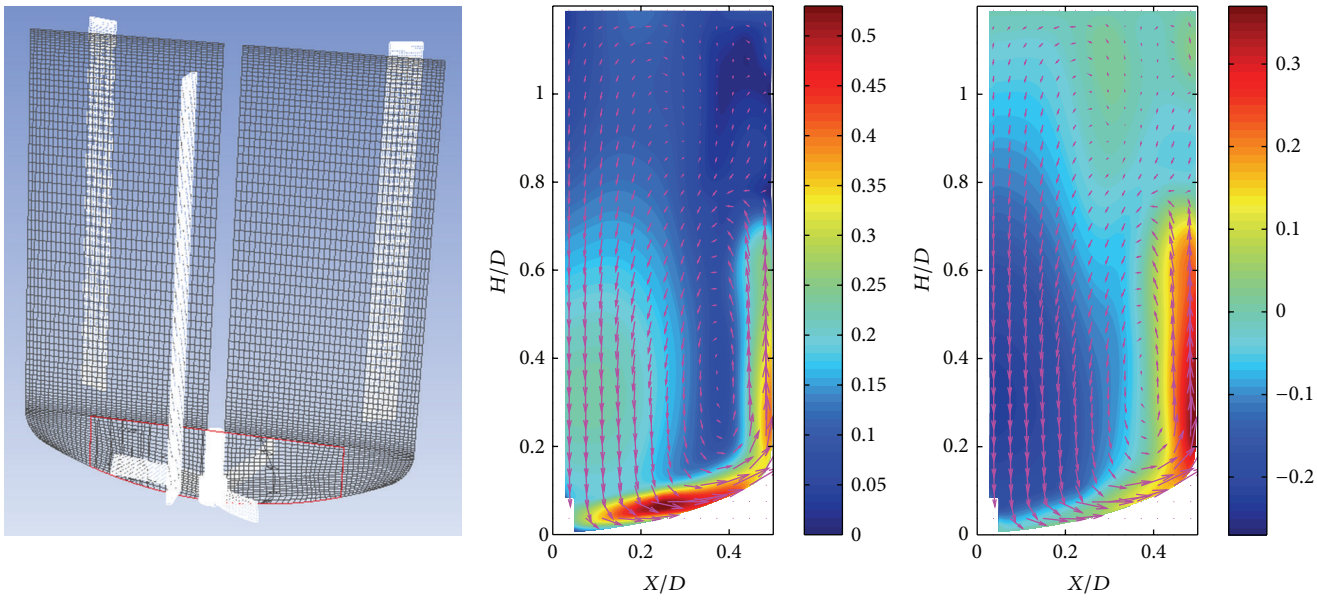

FIGURE 5: numerical model: (a) visualisation of the geometry and the meshing; nondimensional velocity field: (b) mean velocity $\overline{V}/V_{\text{Tip}}$ and (c) axial component V/V_{Tip}.

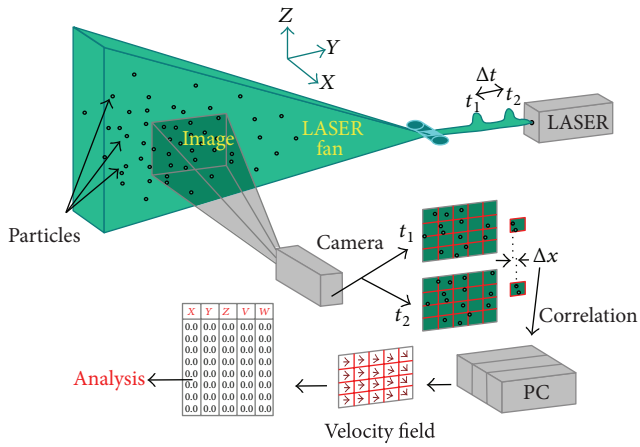

FIGURE 6: PIV method.

fan. A synchronised CCD camera, the axis of which is perpendicular to the illuminated plane, records images resulting from the two LASER pulses. These images contain the particle positions at t and $t + \Delta t$. To compute the local velocity of the particles, the plane is divided in small zones (interrogation zones). A cross correlation is then applied on the two images to compute the mean displacement of the particles inside the different zones. Local velocities of the fluid can thus be computed in the plane [19]. With the 2D PIV method, only the radial and axial velocity components can be measured. To get the third velocity component (tangential), two cameras placed at different angles relative to the illuminated plane can be used to follow stereoscopically the displacement of the particles in the plane. This method is the 3D PIV technique [19].

The 3D PIV technique has been used on the 70 L pilot tank to obtain velocity fields of the flow. Velocity fields were measured with a spatial resolution of 2 mm. An average is then realised on 500 instantaneous velocity fields to obtain mean velocity fields comparable to the velocity fields simulated with the CFD model. This average was performed on a great number of images to obtain converged mean local velocities (Figure 7), avoiding the influence of the position of the impeller (phase).

Due to the fact that PIV is an optical technique, geometrical configuration of the stirred tank may induce disturbance on the measured flow field. In Figure 7, one may see baffles (white vertical lines) and thickness variation of the tank wall (white horizontal lines) which prevent computing accurate values of local velocities in some regions.

In order to validate the k-ε model, simulated axial and radial velocity profiles normalised by the Tip speed value (V_{Tip}) have been compared to experimental ones. To reduce the experimental fluctuation errors, these profiles have been obtained by averaging five non-dimensional velocity fields obtained at five agitation speeds (50, 60, 70, 80, and 90 RPM). Figures 8(a) and 8(b), respectively, represent axial and radial normalised profiles of the mean velocity (V) and of the three components of the velocity: axial (V), radial (U), and tangential (W). Axial profiles have been computed along four vertical lines situated between the agitation axis and the vertical wall of the tank ($X/D = 0.5$) whereas radial profiles have been computed at half-height of the tank ($Z/D = 0.5$). These profiles show that CFD results are in good agreement with experimental PIV results. The maximum prediction error between the PIV measurements and CFD prediction is about 10% within the experimental error (~10%). The CFD

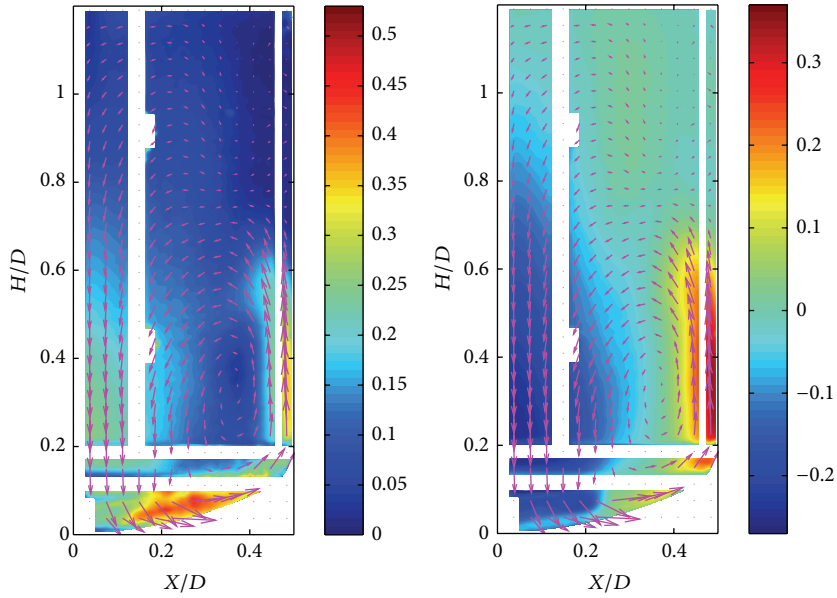

FIGURE 7: 3D PIV nondimensional velocity field: (a) mean velocity $\overline{V}/V_{\text{Tip}}$ and (b) axial component V/V_{Tip}.

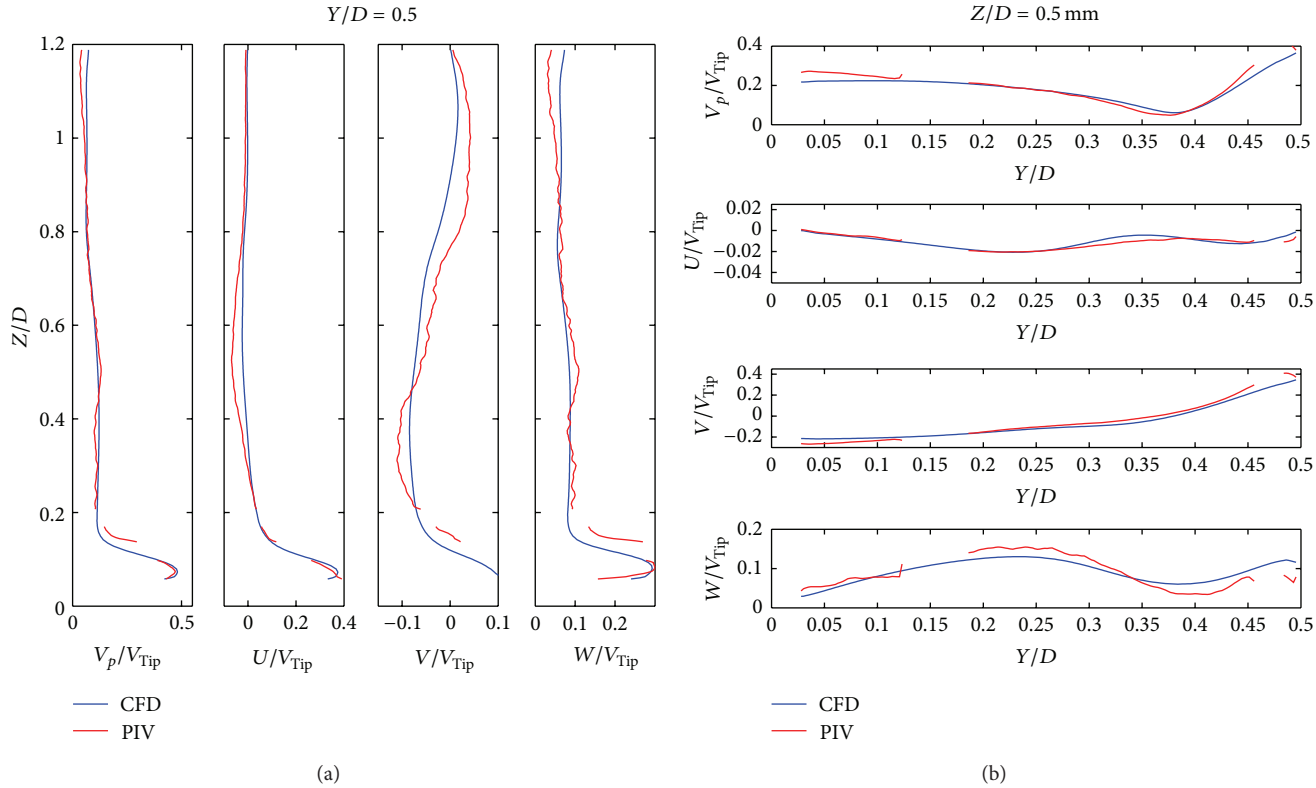

FIGURE 8: (a) axial and (b) radial evolution of non-dimensional mean velocity (V) and the three non-dimensional components of the velocity: axial (V), radial (U), and tangential (W).

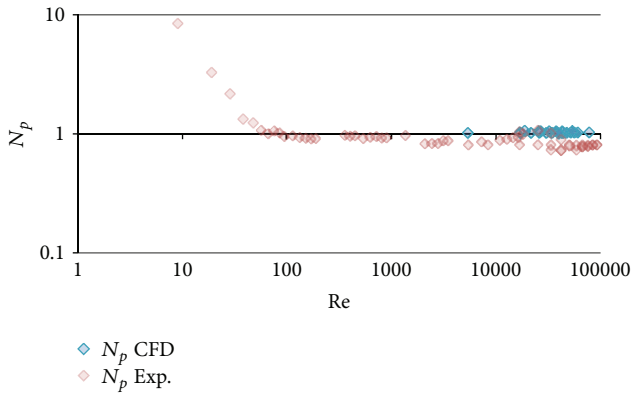

Figure 9: Power Number comparison.

model is thus able to provide representative values of the flow hydrodynamic quantities.

The CFD simulation results have been further validated by experimental measurement of the power number. The power number is deduced from the torque C measured or computed on the impeller axis and blades as follows:

$$P = 2\pi NC,$$
$$Np = \frac{P}{\rho N^3 d^5}. \quad (5)$$

The experimental torque has been measured with a torque meter installed on the agitation motor in the 70 L tank with several liquids of different viscosities in order to cover Reynolds number ranging from 10 to 10^5. The numerical torque is computed from CFD simulations on the impeller and the agitation axis.

Comparison of the experimental and simulated power numbers is presented in Figure 9. These results show that the computed power number is greater than the experimental one due to the use of a moving wall at the bottom of the tank but remained in the same range, within the experimental error. The CFD model is then able to predict the power consumption in the turbulent regime (Re $>$ 10^4). On this figure, one can see that, in this geometry, the power number remained constant with the Reynolds in both transitional and turbulent regimes (Re $> 10^3$).

3.3. Modelling the Solid Suspension Behaviour. Assuming that the solid particles have a negligible influence on the fluid flow (volume fraction less than 0.1%), the Eulerian Mixture model is implemented to the previously computed k-ε model. Only drag force is considered in the interphase momentum exchange term with the Schiller-Naumann's drag correction available for spherical particles.

In order to compare experimental Nhs values to computed ones, we considered that the computed homogeneous suspension is reached when the local solid volume fraction reaches ±2% of its averaged value ($0.74\,\mathrm{cm^3 \cdot L^{-1}}$) within 95% of the whole tank volume. To obtain a representative model of the experimental observation, the impeller speed is set to the experimental value of Nhs, 20 RPM, while the particle equivalent diameter is fitted until the criterion of homogeneous suspension is reached.

In Figure 10(a), the spatial distribution of the solid volume fraction is computed on a vertical plan for an agitation speed of 20 RPM and a particle equivalent diameter of 7 μm. For this equivalent diameter, integration of the local solid volume fraction on the entire volume shows that the suspension reaches the homogeneous criterion ($0.74\,\mathrm{cm^3 \cdot L^{-1}} \pm 2\%$) in more than 95% of the whole tank volume (Figure 10(b)). The model is thus representative of the experimental observations for a particle equivalent diameter equal to 7 μm.

This adjusted value of the particle diameter is very close to the value measured by granulometry inside the stirred cell (Figure 2). According to these results, one may conclude that hydrodynamic conditions reached at Nhs are sufficient to avoid the formation of aluminium salts aggregates.

4. Results and Discussion

The numerical model of the solid suspension has been used to determine Nhs at three different scales in geometrically similar stirred tanks, the volume of which were 12.5 L, 70 L, and 375 L. Results are presented in Figure 11 (green circles). In order to reduce computing time, homogeneous suspension speed has been computed with an accuracy of 2.5 RPM. Experimental measurement of Nhs has also been performed at the same scales (blue marks). Results from CFD are in very good agreement with those experiment results.

Based on the literature [20], extrapolation of the just-suspended speed (Njs) can be performed according to two criteria: if the regime is controlled by the particle lift from the tank bottom, conservation of the Tip speed will be chosen as invariant parameter, whereas if the regime is controlled by the particle deposition on the tank bottom, the invariant parameter will be the volumetric power consumption. In the case of solid suspension denser than the working fluid, the process is controlled by sedimentation which can be expressed by analogy, as deposition. According to this analogy, a model based on the conservation of the volumetric power consumption will be able to predict Nhs at different scales as it is shown in Figure 11 (red curve). The CFD calculations have not been performed for Reynolds number lower than $8 \cdot 10^3$ because the k-ε model is only suited for fully developed turbulent regime. However, as shown in Figure 9, experimental study of the power consumption has shown that the power number remained constant in the transitional regime (Re $>$ 10^3). Consequently, Nhs has been measured at four different scales for Reynolds number lower than $8{\cdot}10^3$ to evaluate the sensibility of the model in the transitional regime. These results show that the model is well suited to predict Nhs in the transitional regime as long as the power number is constant in this regime.

5. Conclusions

In this work, a CFD calculation was successfully used to model the global behaviour of a complex solid suspension. Turbulent flow inside the stirred tank was first simulated using the k-ε model and the results have been validated by experimental PIV measurements. In order to model the

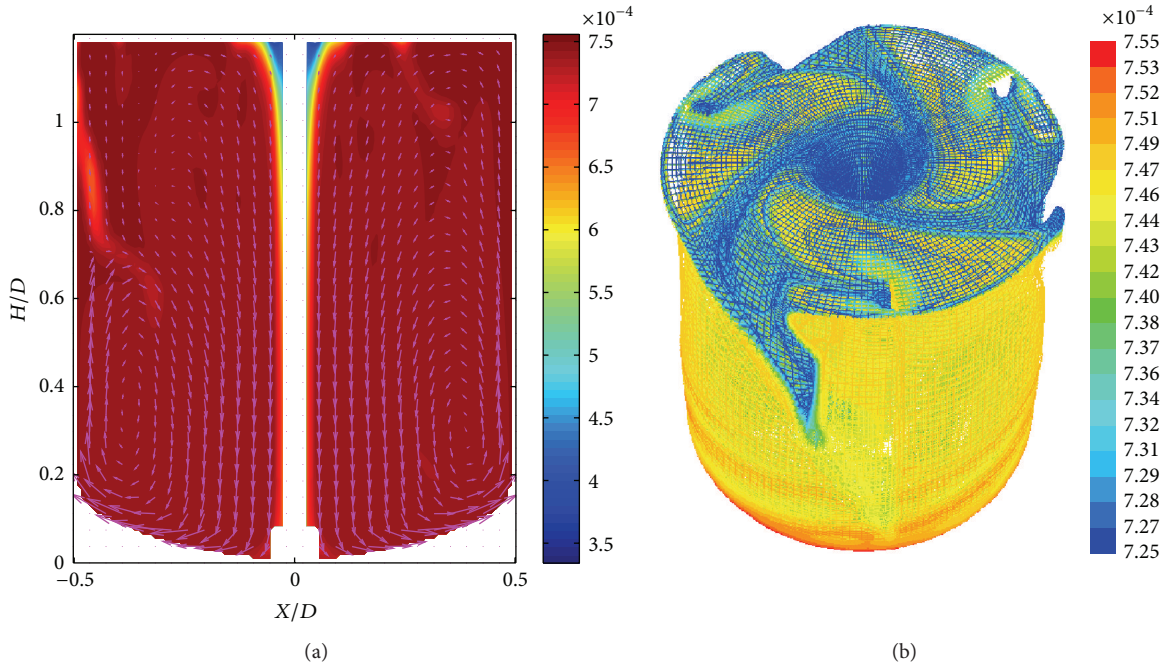

(a) (b)

Figure 10: Spatial distribution of the computed solid volume fraction: (a) on a vertical plan and (b) within the whole volume.

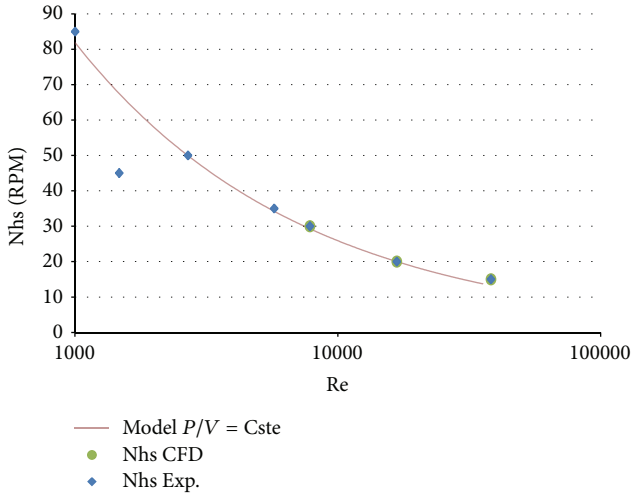

Figure 11: Estimation of Nhs at different scales.

solid suspension, the "Eulerian Mixture" model was then implemented in the previous model, assuming that due to the low concentration and to the very small size of particles, the solid phase would not affect the fluid flow. The equivalent diameter of the particles has been fitted inside the model to be representative of the experimental observations of the homogeneous suspension. Value of this diameter was then successfully compared to the value measured by granulometry under agitation. This result shows that the conditions needed to reach homogeneous suspension inside the tank avoid the formation of aggregates.

Finally, the model was used to compute Nhs at different scales. Corresponding results were successfully compared to Nhs values experimentally measured at the same scales.

These results allow the conclusion that the homogeneous suspension speed Nhs is directly correlated to the volumetric power consumption and that these quantities could thus be chosen as an invariant parameter in scale-up or scale-down operations.

References

[1] E. L. Paul, V. A. Atiemo-Obeng, and S. M. Kresta, *Handbook of Industrial Mixing*, John Wiley & Sons, Hoboken, NJ, USA, 2010.

[2] R. Jafari, J. Chaouki, and P. A. Tanguy, "A comprehensive review of just suspended speed in liquid-solid and gas-liquid-solid stirred tank reactors," *International Journal of Chemical Reactor Engineering*, vol. 10, no. 1, article R1, 2012.

[3] F. Ricard, C. Brechtelsbauer, X. Y. Xu, and C. J. Lawrence, "Monitoring of multiphase pharmaceutical processes using electrical resistance tomography," *Chemical Engineering Research and Design*, vol. 83, no. 7 A, pp. 794–805, 2005.

[4] T. N. Zwietering, "Suspending of solid particles in liquid by agitators," *Chemical Engineering Science*, vol. 8, no. 3-4, pp. 244–253, 1958.

[5] R. Angst and M. Kraume, "Experimental investigations of stirred solid/liquid systems in three different scales: particle distribution and power consumption," *Chemical Engineering Science*, vol. 61, no. 9, pp. 2864–2870, 2006.

[6] R. Jafari, P. A. Tanguy, and J. Chaouki, "Experimental investigation on solid dispersion, power consumption and scale-up in moderate to dense solid-liquid suspensions," *Chemical Engineering Research and Design*, vol. 90, no. 2, pp. 201–212, 2012.

[7] S. Wang, D. V. Boger, and J. Wu, "Energy efficient solids suspension in an agitated vessel-water slurry," *Chemical Engineering Science*, vol. 74, pp. 233–243, 2012.

[8] J. Aubin, D. F. Fletcher, and C. Xuereb, "Modeling turbulent flow in stirred tanks with CFD: the influence of the modeling approach, turbulence model and numerical scheme," *Experimental Thermal and Fluid Science*, vol. 28, no. 5, pp. 431–445, 2004.

[9] D. A. Deglon and C. J. Meyer, "CFD modelling of stirred tanks: numerical considerations," *Minerals Engineering*, vol. 19, no. 10, pp. 1059–1068, 2006.

[10] A. Delafosse, A. Line, J. Morchain, and P. Guiraud, "LES and URANS simulations of hydrodynamics in mixing tank: comparison to PIV experiments," *Chemical Engineering Research and Design*, vol. 86, no. 12, pp. 1322–1330, 2008.

[11] B. N. Murthy and J. B. Joshi, "Assessment of standard $k-\varepsilon$, RSM and LES turbulence models in a baffled stirred vessel agitated by various impeller designs," *Chemical Engineering Science*, vol. 63, no. 22, pp. 5468–5495, 2008.

[12] G. R. Kasat, A. R. Khopkar, V. V. Ranade, and A. B. Pandit, "CFD simulation of liquid-phase mixing in solid-liquid stirred reactor," *Chemical Engineering Science*, vol. 63, no. 15, pp. 3877–3885, 2008.

[13] G. Montante, G. Micale, F. Magelli, and A. Brucato, "Experiments and CFD predictions of solid particle distribution in a vessel agitated with four pitched blade turbines," *Chemical Engineering Research and Design*, vol. 79, no. 8, pp. 1005–1010, 2001.

[14] G. Micale, F. Grisafi, L. Rizzuti, and A. Brucato, "CFD simulation of particle suspension height in stirred vessels," *Chemical Engineering Research and Design*, vol. 82, no. 9, pp. 1204–1213, 2004.

[15] A. R. Khopkar, G. R. Kasat, A. B. Pandit, and V. V. Ranade, "Computational fluid dynamics simulation of the solid suspension in a stirred slurry reactor," *Industrial and Engineering Chemistry Research*, vol. 45, no. 12, pp. 4416–4428, 2006.

[16] G. Micale, G. Montante, F. Grisafi, A. Brucato, and J. Godfrey, "CFD simulation of particle distribution in stirred vessels," *Chemical Engineering Research and Design*, vol. 78, no. 3, pp. 435–444, 2000.

[17] D. Wadnerkar, R. P. Utikar, M. O. Tade, and V. K. Pareek, "CFD simulation of solid-liquid stirred tanks," *Advanced Powder Technology*, vol. 23, no. 4, pp. 445–453, 2012.

[18] R. H. Perry and D. Green, *Chemical Engineer's Handbook*, McGraw-Hill, New York, NY, USA, 1984.

[19] M.-L. Collignon, *Étude de l'hydrodynamique au sein d'un bioréacteur à cuve agitée utilise pour la culture de cellules animales adhérentes sur microporteurs: caractérisation expérimentale et théorique des écoulements via des outils eulériens et lagrangiens [Ph.D. report]*, 2012.

[20] C. Xuereb, M. Poux, and J. Bertrand, *Agitation et Mélange: Aspects Fondamentaux et Applications Industrielles, L'Usine Nouvelle*, Dunod, Paris, France, 2006.